

## RESEARCH ARTICLE

# Improved Framework for Tractography Reconstruction of the Optic Radiation

Eloy Martínez-Heras<sup>1</sup>, Federico Varriano<sup>2</sup>, Vesna Prćkovska<sup>1</sup>, Carlos Laredo<sup>3</sup>, Magí Andorrà<sup>1</sup>, Elena H. Martínez-Lapiscina<sup>1</sup>, Anna Calvo<sup>4</sup>, Erika Lampert<sup>1</sup>, Pablo Viloslada<sup>1</sup>, Albert Saiz<sup>1</sup>, Alberto Prats-Galino<sup>2</sup>, Sara Llufriu<sup>1\*</sup>

**1** Center of Neuroimmunology, Service of Neurology, Hospital Clinic and Institut d'Investigacions Biomèdiques August Pi i Sunyer (IDIBAPS), Barcelona, Spain, **2** Laboratory of Surgical NeuroAnatomy (LSNA), Facultat de Medicina, Universitat de Barcelona, Barcelona, Spain, **3** Comprehensive Stroke Center, Department of Neuroscience, Hospital Clinic and Institut d'Investigacions Biomèdiques August Pi i Sunyer (IDIBAPS), Barcelona, Spain, **4** Medical Imaging Platform, Institut d'Investigacions Biomèdiques August Pi i Sunyer (IDIBAPS), Barcelona, Spain

\* [SLLUFRIU@clinic.ub.es](mailto:SLLUFRIU@clinic.ub.es)



CrossMark  
click for updates

## Abstract

### OPEN ACCESS

**Citation:** Martínez-Heras E, Varriano F, Prćkovska V, Laredo C, Andorrà M, Martínez-Lapiscina EH, et al. (2015) Improved Framework for Tractography Reconstruction of the Optic Radiation. PLoS ONE 10(9): e0137064. doi:10.1371/journal.pone.0137064

**Editor:** Christophe Lenglet, University of Minnesota, UNITED STATES

**Received:** December 16, 2014

**Accepted:** August 12, 2015

**Published:** September 16, 2015

**Copyright:** © 2015 Martínez-Heras et al. This is an open access article distributed under the terms of the [Creative Commons Attribution License](#), which permits unrestricted use, distribution, and reproduction in any medium, provided the original author and source are credited.

**Data Availability Statement:** Image datasets will be available after acceptance at <http://www.neuroimmunologybcn.org/projects>.

**Funding:** This work was partially funded by a donation from the Asociación Esclerosis Múltiple Isla de Menorca (AEMIM, <http://www.esclerosismultiple.com>) to AS. It was also funded by the FP7 Marie Curie Intra-European Fellowship, project acronym: ConnectMS, project number: 328060 to VP. The funders had no role in study design, data collection and analysis, decision to publish, or preparation of the manuscript.

The optic radiation (OR) is one of the major components of the visual system and a key structure at risk in white matter diseases such as multiple sclerosis (MS). However, it is challenging to perform track reconstruction of the OR using diffusion MRI due to a sharp change of direction in the Meyer's loop and the presence of kissing and crossing fibers along the pathway. As such, we aimed to provide a highly precise and reproducible framework for tracking the OR from thalamic and visual cortex masks. The framework combined the generation of probabilistic streamlines by high order fiber orientation distributions estimated with constrained spherical deconvolution and an automatic post-processing based on anatomical exclusion criteria (AEC) to compensate for the presence of anatomically implausible streamlines. Specifically, those ending in the contralateral hemisphere, cerebrospinal fluid or grey matter outside the visual cortex were automatically excluded. We applied the framework to two distinct high angular resolution diffusion-weighted imaging (HARDI) acquisition protocols on one cohort, comprised of ten healthy volunteers and five MS patients. The OR was successfully delineated in both HARDI acquisitions in the healthy volunteers and MS patients. Quantitative evaluation of the OR position was done by comparing the results with histological reference data. Compared with histological mask, the OR reconstruction into a template (OR-TCT) was highly precise (percentage of voxels within the OR-TCT correctly defined as OR), ranging from 0.71 to 0.83. The sensitivity (percentage of voxels in histological reference mask correctly defined as OR in OR-TCT) ranged from 0.65 to 0.81 and the accuracy (measured by F1 score) was 0.73 to 0.77 in healthy volunteers. When AEC was not applied the precision and accuracy decreased. The absolute agreement between both HARDI datasets measured by the intraclass correlation coefficient was 0.73. This improved framework allowed us to reconstruct the OR with high reliability and accuracy independently of the acquisition parameters. Moreover, the reconstruction was possible even in

**Competing Interests:** EMH, FV, VP, CL, MA, EHM, AC, EL, APG, and SL have declared that no competing interests exist. P. Villoslada received compensation for advisory from Roche, Novartis and Bionure Incorporation. AS received compensation for advisory and speaking from Bayer-Schering, Merck-Serono, Biogen-Idec, Sanofi-Aventis, Teva Pharmaceutical Industries Ltd and Novartis. This does not alter the authors' adherence to PLOS ONE policies on sharing data and materials. Dr. Pablo Villoslada, coauthor of the paper, is a PLOS ONE Editorial Board member. This does not alter the authors' adherence to PLOS ONE editorial policies and criteria.

the presence of tissue damage due to MS. This framework could also be applied to other tracts with complex configuration.

## Introduction

Diffusion-weighted imaging (DWI) is a magnetic resonance imaging (MRI) modality that measures the amount and directionality of water molecule diffusion within tissue [1]. From DWI, the direction of maximal diffusivity along axonal fibers can be estimated for each voxel. This information enables the reconstruction of the architectural configuration of white matter (WM) trajectories between regions of interest (ROIs) through fiber tractography [2]. Detailed tractography studies have created virtual anatomic atlases of WM connections in the human brain [3, 4] that agree with results from dissection and tracer studies [5, 6]. However, fiber tracking has several limitations that may affect the reliability and reproducibility of outcomes resulting from different approaches. First, the image resolution in diffusion MRI (dMRI) is usually several orders of magnitude higher than the actual axons size, so each voxel contains information from hundreds of thousands of axon fibers [7]. Moreover, the presence of crossing fibers, highly curved or diverging fiber bundles, might affect the directionality of each fiber bundle within the voxel [8]. The selection and positioning of the specific seed ROIs used to perform the tractography may lead to considerable variability in the results [9]. In addition, several tractography algorithms are available; the two main distinguishing factors relate to how WM fiber tracts are modeled within a voxel and how the tracts are reconstructed [10]. Deterministic streamline tractography is primarily based upon streamline algorithms in which the local tract direction is defined by the major eigenvector of the diffusion tensor and can produce anatomically faithful reconstructions of WM fascicules. However, in general, branching will not be represented and this approach may be less effective in regions where considerable fiber crossing is present and curvature is high [11]. Probabilistic tractography algorithms based on a fiber orientation density function provide information about the confidence that one can assign to a reconstructed trajectory and can indicate the occurrence of branching [12]. The high-order tractography model, constrained spherical deconvolution (CSD), is advisable for performing a robust tractography [13]. Deterministic tractography can also be estimated from the fiber orientation distribution (FOD) and obtain robust tracking in the presence of crossing fibers. However, deterministic tractography with high order models is prone to missing existing streamlines [14]. The use of high order integration over fiber orientation distributions (iFOD2) [15] derived from CSD could improve tracking in regions containing complex fiber architecture [16]. Unfortunately, probabilistic fiber tracking frequently generates anatomically implausible streamlines. New methods based on anatomical information from whole-brain tractography, such as anatomically-constrained tractography (ACT) [17], have been developed to provide a more biologically accurate reconstruction through dynamic thresholding strategy. However, this method does not resolve the problem of false positives and systematic errors in the tractography. For that reason, we propose the use of post-processing based on anatomical exclusion criteria (AEC) to define the final tracking results and exclude aberrant streamlines.

The optic radiation (OR) is one of the major components of the human visual system. It links the lateral geniculate nucleus (LGN) with the visual cortex and is one of the most difficult tracts to reconstruct with dMRI-based methods [18] due to a sharp change of direction in the Meyer's loop and the presence of kissing and crossing fibers along the pathway [19]. The topography of the OR is evident in histological sections [20], however, the reconstruction of

the OR in vivo suffers from inaccuracy and different levels of success have been reported [21, 22]. Variability in the results may derive from a lack of consistency in the selection of the seed regions and tractography algorithms (deterministic and probabilistic) used for fiber tractography [23, 24] as well as in the selection or exclusion of streamlines representing the OR [25]. To reconstruct the OR through tractography some authors have placed a waypoint seed distal to the Meyer's loop in order to map the rapidly curving anterior fibers [26–29] while few studies have been able to obtain the OR from LGN seeds [19, 30, 31]. Although most techniques succeeded in representing the simplest anterior-posterior streamlines of the OR, aberrant fibers were eliminated by visual inspection [32] or by looking at the anatomical plausibility of the highest scoring pathways [33]. These approaches can induce biases in the position, shape, size and length of the streamline distribution [34] and do not ensure the representation of the most reliable pathway based on neuroanatomical knowledge.

The OR can be damaged in diseases such as multiple sclerosis (MS). The visual pathway can be used to evaluate the interplay of different mechanisms of damage in MS such as inflammation (lesions and normal appearing WM), demyelination and axonal damage and also particular mechanisms such as trans-synaptic degeneration [35–38]. The presence of lesions with low fractional anisotropy can erroneously terminate the tracking algorithm from conventional DTI-tractography or cause a deviation of the streamlines at the level of the lesions [39]. As such, an accurate and reproducible reconstruction of the OR and other tracts is essential to evaluate the consequences of WM damage in MS or other neurological diseases, and for surgery planning [24].

The purpose of this article is to introduce an improved tractography framework to reconstruct the OR using the thalamus and visual cortex as seed and target masks that combines probabilistic streamline fiber tracking by iFOD2 and automatic post-processing based on AEC. We aim to demonstrate its precision, accuracy and reproducibility in two different single-shell high angular resolution diffusion-weighted imaging (HARDI) datasets from healthy volunteers and explore its applicability in the presence of tissue damage caused by MS.

## Materials and Methods

### Material and Imaging

Ten healthy volunteers and five patients with MS were recruited for this study. The included healthy volunteers [3 male and 7 female, mean (SD) age 30 ( $\pm 8$ ) years] did not have any known neurological or psychiatric diseases. The MS patients [2 male and 3 female, mean (SD) age 35 ( $\pm 9$ ) years] were recruited from the MS Unit at the Hospital Clinic in Barcelona. The Ethics Committee of Hospital Clinic of Barcelona approved the study and a signed consent form was obtained from all the participants.

### MRI data acquisition

MRI images were acquired on a 3T Magnetom Trio (Siemens, Erlangen, Germany) scanner, using a thirty-two channel phased-array head coil. One 3D T1-weighted structural and two different DWI sequences were acquired in the same scanning session. The 3D-structural image was a T1-weighted MPRAGE sequence with the following acquisition parameters: TR: 2050 ms, TE: 2.41 ms TI: 1050 ms, flip angle: 9°, 192 contiguous sagittal slices with 0.86 x 0.86 x 0.9 mm<sup>3</sup> voxel size, 256 x 256 matrix size. Two HARDI datasets were acquired, HARDI A: TR/TE, 16600/110 ms; acquisition matrix, 154 x 154; 100 contiguous axial slices; 1.5 mm isotropic voxel size; b value, 1500 s/mm<sup>2</sup>; 16 minutes acquisition time and HARDI B: TR/TE, 6200/84 ms; acquisition matrix, 96 x 96; 55 contiguous axial slices; 2.5 mm isotropic voxel size; b value, 1000 s/mm<sup>2</sup>; 4 minutes acquisition time. Both HARDI datasets used the same 60 numbers of

gradient directions [40] and a single baseline image acquired at  $0\text{ s/mm}^2$ . Parallel imaging was applied with a geometric reduction factor of 2 to reduce the distortion caused by susceptibility differences at tissue interfaces. In addition, a 2D field map sequence was acquired to correct geometric distortions of the DWI caused by susceptibility differences between air-bone or air-tissue interfaces. The field map was obtained at two different echo times ( $TE_1 = 4.92\text{ ms}$  and  $TE_2 = 7.38\text{ ms}$ ) and in the same slice prescription, slice thickness and field of view as both HARDI datasets.

### Construction and inspection of seed and target masks

The 3D-structural image served as an anatomical landmark to obtain GM ROIs in each hemisphere. The parcellation scheme from Freesurfer (FS) software [41] was used as a first approximation to outline the thalamus and visual cortex that were going to serve as the seed and target masks, respectively. In patients, the 3D-structural image was also used to manually create a lesion mask with the ITK-SNAP toolkit [42]. Afterwards, an automated lesion filling was applied to the 3D-structural image to improve segmentation and registration steps in patients [43]. The seed and target masks were then further inspected and corrected by an experienced neuroanatomist using AMIRA 5.1 software (Mercury Computer Systems, Berlin, Germany) to reduce inaccuracies and limitations of the parcellation algorithm. The thalamus seed mask used in this study corresponds to the Thalamus-Proper parcellation in the Desikan-Killiany Atlas while the visual cortex target mask was obtained by merging the pericalcarine, cuneus, lateraloccipital, lingual and precuneus parcellations. As the LGN was not properly parcellated in the thalamus-proper ROI, we manually selected and included this nucleus in the seed mask.

### Proposed framework to reconstruct the OR

The schematic diagram of the framework is presented in Fig 1. Initially, we performed standard preprocessing of the DWIs that included geometric distortion correction for echo planar images (EPI) with fieldmap images and head motion correction. Fieldmap-based unwarping of the EPI was done using PRELUDE to unwrap the phase and FUGUE to compute the distortion by means of FMRIB Software Library (FSL, <http://www.fmrib.ox.ac.uk/fsl>) [44]. After applying eddy current corrections we rotated the gradient vectors in both HARDI datasets in order to compensate for head motion. This was followed by the registration of the structural images to the corresponding HARDI dataset using the Boundary-Based-Registration method [45]. Probabilistic tractography from seed to target masks was performed in each hemisphere using the MRtrix3 package (<https://github.com/jdtournier/mrtrix3>) [46]. A set of 100,000 streamlines was generated from the seed mask in only one direction and stopped as soon as it entered the target mask. The default step size, curvature and FOD amplitude threshold (0.1) were used. We applied probabilistic streamline fiber tracking by iFOD2 derived from CSD with a maximum harmonic order of 8 [47, 48], and used FreeSurfer tissue segmentations for ACT. Anatomically unrealistic streamlines were present in the final tracking results. To correct for this problem, we automatically applied AEC to the results. We first converted the tract file into a track density image at native resolution based on the map of the fraction of tracks that enter each voxel. We set a threshold of 1% of the maximum value included in the track density image [32, 49] and selected the biggest cluster in order to get a temporary tract. The temporary tract file retained plausible streamlines that connected the seed mask to the target mask and removed streamlines of low confidence, i.e. false positives. Second, we applied a binary exclusion mask to the temporary tract file comprised of the cerebrospinal fluid (CSF), whole contralateral hemisphere and ipsilateral GM regions that did not include the seed and target masks. As a result, any streamline crossing the midline or reaching cortical and subcortical GM regions

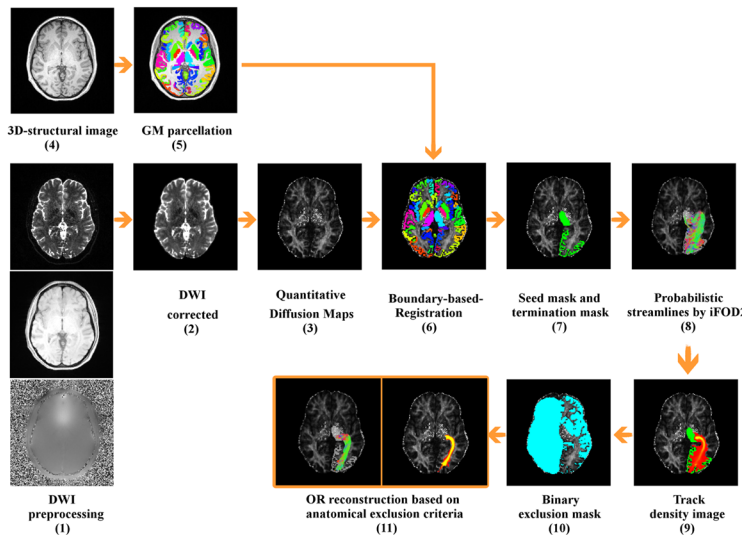


**Fig 1. Tractography reconstruction framework of the optic radiations.** (1) Standard preprocessing of the DWIs including Echo Planar Imaging distortion correction, eddy current distortion correction and head motion correction. (2) Distortion correction of the DWI. (3) Quantitative diffusion fractional anisotropy (FA) mapping. (4-5) Subcortical segmentation and cortical parcellation from FS of the 3D-structural image. (6) Registration of the structural images to the corresponding DWI sequence. (7) Seed and target masks. (8) Probabilistic streamline fiber tracking by high order integration over fiber orientation distributions (iFOD2) derived from constrained spherical deconvolution (CSD) with a maximum harmonic order of 8 and use of ACT during tracking. (9) Conversion of the tract file into a track density image. (10) Exclusion mask comprising CSF, whole contralateral hemisphere and ipsilateral GM regions. (11) Final optic radiation reconstruction in track density image and 3D tract file.

doi:10.1371/journal.pone.0137064.g001

outside the seed and target masks were excluded. Next, we converted the tract file back into a track density image and the resulting images were scaled to a range of [0–1] [50] to enable the comparison between individual samples. In patients with MS we overlaid the lesion mask obtained with ITKsnap on the reconstructed OR to identify how many patients presented lesions at that level.

In order to compare our framework with conventional DTI-tractography, we performed the same pre-processing and applied deterministic fiber tracking based on the fiber assignment by continuous tracking (FACT) [51] method in the healthy volunteers with the same seed and target mask. This fiber tracking was done with MRtrix3 software using the default setting parameters and an FA threshold of 0.1.

### Qualitative and quantitative evaluation of the method

Visual inspection of the OR resulting from streamlines in both HARDI datasets was performed by a neuroanatomy specialist to evaluate concordance in morphology and position with the known anatomical description of this pathway [52]. Quantitative evaluation of the OR position was done by comparing the results with histological reference data of the OR [20, 53]. The OR obtained in each HARDI dataset was converted into a template (tractography-constructed template, OR-TCT) ([S1 File](#)). To do so, each individual track density image was aligned to the highest resolution sequence (HARDI A) and was normalized into a standardized space (Montreal Neurological Institute, MNI152) and then averaged. The histological reference data was edited to exclude GM and CSF regions from the MNI152 structural template image in order to preserve only WM regions. It was then converted to a binary mask to incorporate the

information of all the subjects included in the histological atlas. The sensitivity, precision, specificity and F-measure of our method were calculated in each HARDI dataset to assess the similarities between the OR-TCT and the histological reference data.

Sensitivity was measured as the proportion of voxels within the reference mask that were correctly defined as OR in the OR-TCT.

$$\text{Sensitivity} = \frac{\text{True positives}}{(\text{True positives} + \text{False negatives})} \quad (1)$$

Specificity was the proportion of voxels outside the reference mask that were correctly classified as non-OR voxels in the OR-TCT.

$$\text{Specificity} = \frac{\text{True negatives}}{(\text{True negatives} + \text{False positives})} \quad (2)$$

Precision was calculated as the proportion of voxels within the OR-TCT that were correctly defined as OR.

$$\text{Precision} = \frac{\text{True positives}}{(\text{True positives} + \text{False positives})} \quad (3)$$

We included the F1 score, a measure of the tests accuracy, in order to estimate the weighted harmonic mean of precision and sensitivity.

$$F_1 = 2 \cdot \frac{\text{Precision} \cdot \text{Sensitivity}}{(\text{Precision} + \text{Sensitivity})} \quad (4)$$

We also performed a quantitative evaluation of the OR in the absence of the AEC. In order to evaluate the reproducibility of the OR reconstruction we compared the results obtained from the two different HARDI datasets in each subject. The agreement in OR volume was evaluated with Bland-Altman plots [54] and the intraclass correlation coefficient (ICC). Considering the well-recognized anatomical differences between left hemisphere (lh) and right hemisphere (rh) [55], we merged comparison from lh and rh into the same analysis. We used SPSS v.18 to construct the Bland-Altman plots and calculate the ICC.

## Results

The proposed framework reconstructed OR fiber tracking in both HARDI datasets in all the healthy volunteers included in the study. The results were visually concordant with the anatomical description of the streamlines ([Fig 2b](#)). The resulting fiber trajectories emerged from the posterior part of the thalamus, including the LGN. A portion of the streamlines looped anterior and laterally around the temporal horn of the lateral ventricle forming the Meyer's loop, where it sharply turned in a posterior direction, while another portion followed a more direct trajectory. The streamlines then followed the curvature of the ventricular atrium and reached the visual cortex. On the contrary, the application of conventional DTI-tractography was unable to solve the complex configuration in the Meyer's loop, generated unrealistic streamlines and in some cases was unable to even produce an OR reconstruction in two subjects (see [Fig 3](#)). Moreover, the results were largely dependent upon the sequence used, with worse reconstruction obtained with HARDI B.

In patients with MS, the OR were also accurately reconstructed with the proposed framework ([Fig 4c](#)) although all the subjects presented lesions within the tracts ([Fig 4a](#)).

The framework provided good anatomical correspondence between the OR-TCT and the histological reference data in healthy volunteers (see [Fig 5](#)). The sensitivity, precision,

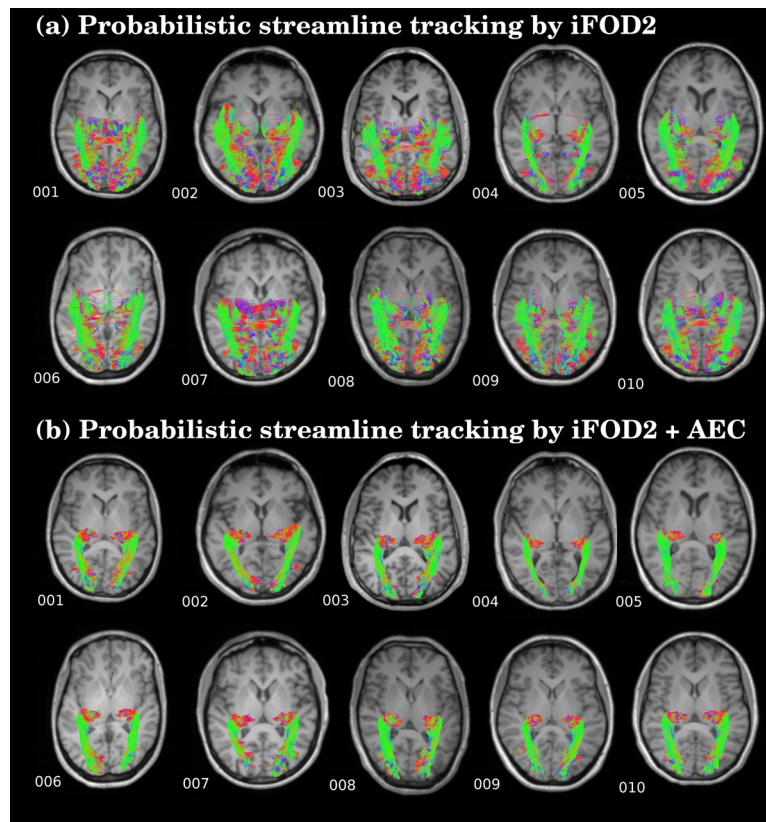


**Fig 2.** Streamlines of the reconstructed OR in ten healthy subjects: (a) Probabilistic streamlines fiber tracking by iFOD2. (b) Probabilistic streamlines fiber tracking by high order integration over fiber orientation distributions (iFOD2) adding the anatomical exclusion criteria (AEC).

doi:10.1371/journal.pone.0137064.g002

specificity and F-measure results are shown in [Table 1](#). The results demonstrate a good match between the OR-TCT in both HARDI datasets and the histological reference mask. Precision ranged from 0.71 to 0.83 depending on the HARDI dataset or hemisphere explored (false positive from 17 to 29%, while accuracy ranged from 0.73 to 0.76. In the HARDI A dataset, with smaller voxel size, the sensitivity was lower than HARDI B while the precision was higher ([Table 1](#)). The application of AEC also increased the precision and accuracy ranges in MS patients ([S1 Table](#)).

When AEC was not applied, streamlines not concordant with prior anatomical knowledge appeared in all subjects (Figs [2a](#) and [4b](#)) and the accuracy of the OR compared to the histological mask decreased (range from 0.25 to 0.33) while sensitivity was very high (range from 0.99 to 1.0) due to the overestimation of WM streamlines with false positives ([Table 1](#)); false positive in non-AEC ranged from 80 to 86% ([S2 Table](#)).

Bland-Altman plots showed good agreement between the OR tracking obtained in both HARDI datasets for all subjects ([Fig 6](#)). We did not detect any outliers, suggesting that the technique is reproducible. The OR was bigger in HARDI B, where voxel size is larger, than in HARDI A ([Table 1](#)) but we did not detect a systematic bias between both images. The ICC measuring the absolute agreement was 0.73 (95% confidence interval: 0.50 to 0.86,  $p < 0.001$ ).

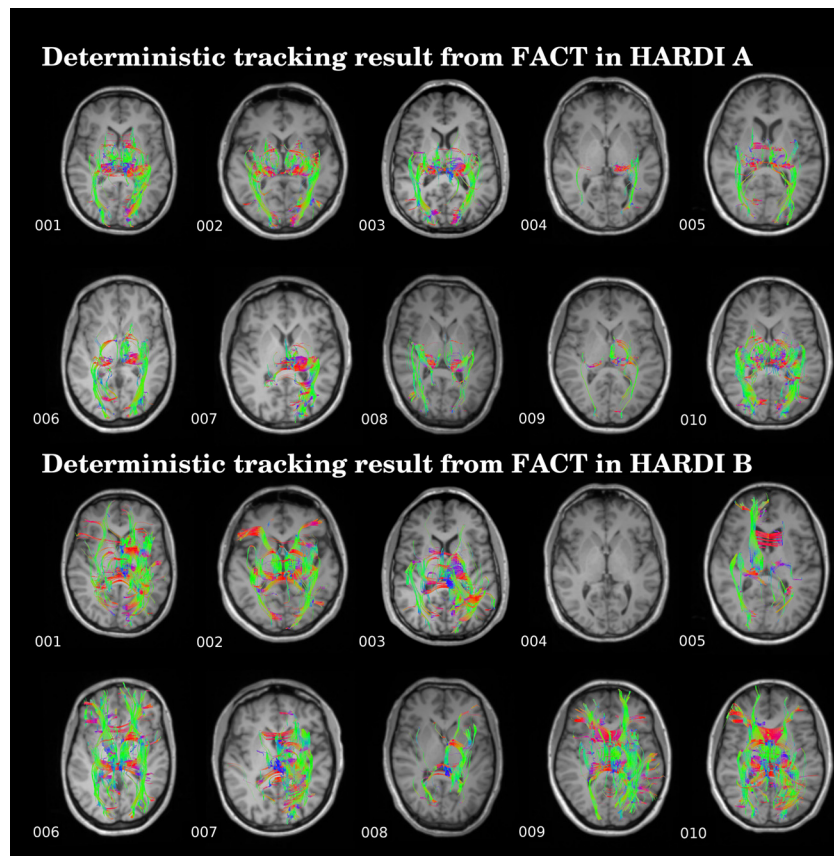


**Fig 3. Deterministic DTI tractography based on fiber assignment by continuous tracking (FACT) in ten healthy subjects in two HARDI datasets.**

doi:10.1371/journal.pone.0137064.g003

## Discussion

We present an improved tractography framework that combines the use of available software packages to reconstruct the OR from thalamus and visual cortex masks with the automatic exclusion of aberrant streamlines through anatomical criteria. Contrary to conventional DTI-tractography this methodology enabled the reconstruction of the whole OR in high concordance with anatomical knowledge and high accuracy in comparison with the histological reference data. In patients with MS, the OR was obtained in all cases even though there were lesions in these areas. Furthermore, this technique was applied in two different HARDI datasets and the resulting OR fiber tracks were comparable, suggesting good reliability of the approach. Our framework used high order probabilistic streamlines derived from CSD and automatic post-processing based on AEC. The AEC steps included the application of a threshold and the selection of the maximally connected volume to retain plausible OR reconstructed streamlines that connect the seed to the target mask. Most widely used methods are based on the application of a threshold to eliminate low probability connections not corresponding to the OR. Another method, ACT, uses information from high-resolution images to decrease the presence of anatomically implausible streamlines generated on fiber tracking. Despite the application of

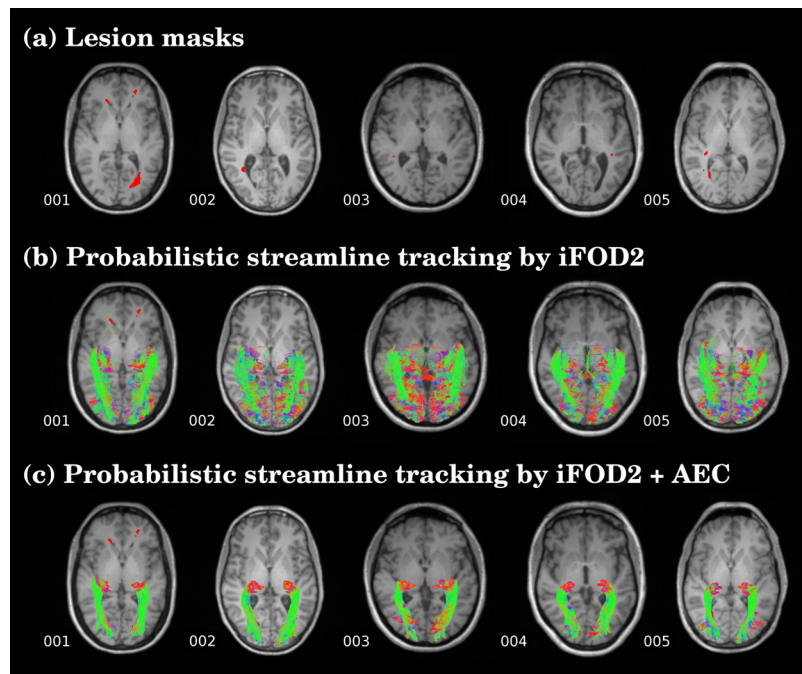


**Fig 4.** Streamlines of the reconstructed OR in five patients with multiple sclerosis: (a) Lesion masks is shown in red. (b) Probabilistic streamlines fiber tracking by iFOD2. (c) Probabilistic streamlines fiber tracking by high order integration over fiber orientation distributions (iFOD2) adding the anatomical exclusion criteria (AEC).

doi:10.1371/journal.pone.0137064.g004

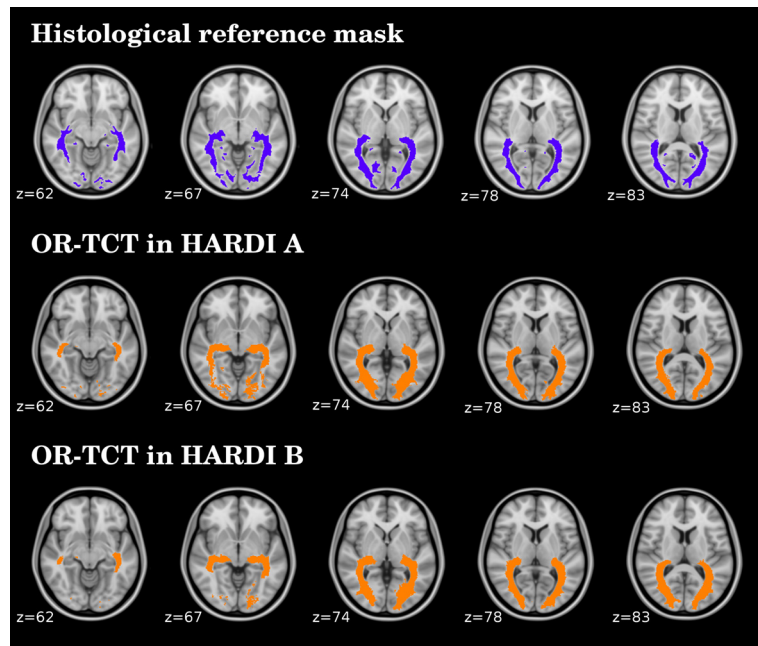


**Fig 5.** Anatomical correspondence between the histological reference mask (in blue color) and tractography-constructed templates (OR-TCT) from both HARDI datasets (in orange color).

doi:10.1371/journal.pone.0137064.g005

**Table 1. Comparison between tractography results and histological reference data in healthy volunteers.**

	OR-TCT (iFOD2)		OR-TCT (iFOD2 + AEC)		reference mask <sup>a</sup>	
	HARDI A <sup>b</sup>	HARDI B <sup>c</sup>	HARDI A <sup>b</sup>	HARDI B <sup>c</sup>		
Tract volume ( $\text{cm}^3$ ), mean ( $\pm \text{SD}$ )	lh rh	44.87 ( $\pm 7.69$ ) 41.69 ( $\pm 8.00$ )	52.38 ( $\pm 14.46$ ) 43.37 ( $\pm 11.03$ )	12.25 ( $\pm 2.73$ ) 12.01 ( $\pm 2.03$ )	16.81 ( $\pm 4.89$ ) 14.99 ( $\pm 3.52$ )	18.4 ( $\pm 2.1$ ) 18.4 ( $\pm 1.3$ )
Sensitivity	lh rh	0.99 0.99	0.99 1.00	0.71 0.65	0.81 0.70	- -
Precision	lh rh	0.18 0.20	0.14 0.17	0.83 0.83	0.71 0.79	- -
Specificity	lh rh	0.92 0.93	0.90 0.92	1.00 1.00	0.99 1.00	- -
F-measure	lh rh	0.30 0.33	0.25 0.29	0.77 0.73	0.76 0.74	- -

<sup>a</sup>Volumes in the histological reference mask were obtained from Clatworthy et al., 2010.

<sup>b</sup>HARDI A: 1.5 mm isotropic voxel size; b-value, 1500  $\text{s/mm}^2$

<sup>c</sup>HARDI B: 2.5 mm isotropic voxel size; b-value, 1000  $\text{s/mm}^2$

#### Abbreviations:

AEC: automatic post-processing based on anatomical exclusion criteria.

iFOD: high order integration over fiber orientation distributions.

lh: left hemisphere.

OR-TCT: optic radiation tractography-constructed template.

rh: right hemisphere.

doi:10.1371/journal.pone.0137064.t001

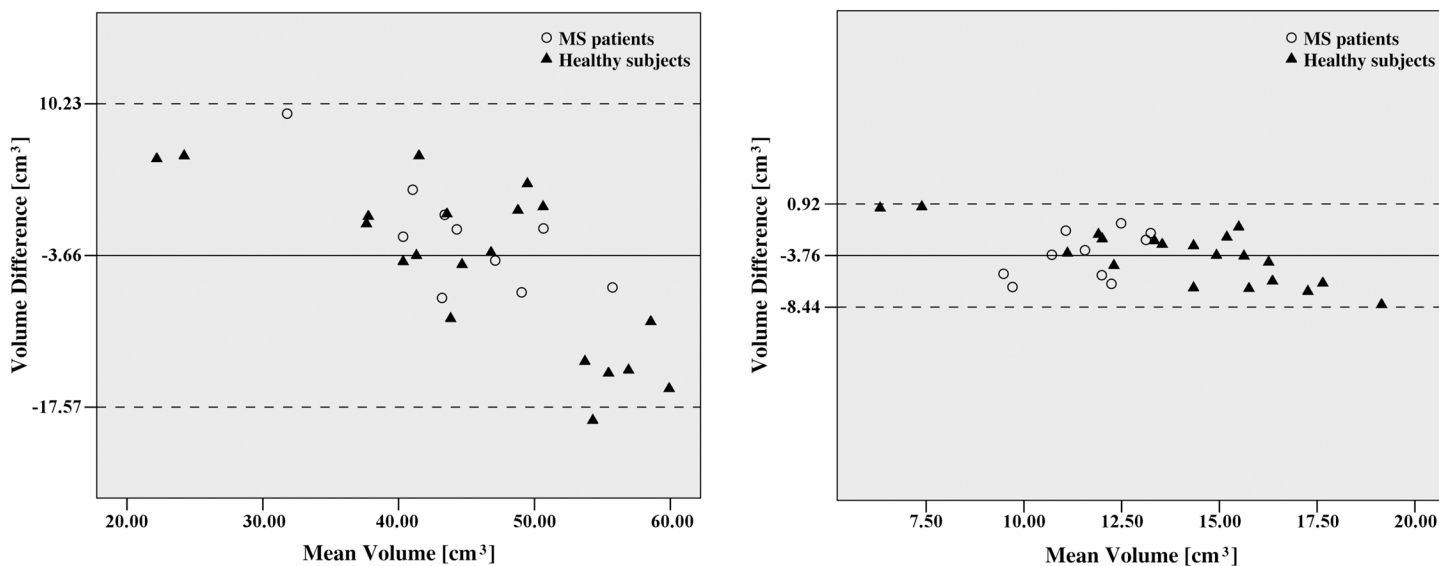


**Fig 6. Bland-Altman plots comparing the mean volume of OR in both HARDI datasets.** Left panel corresponds to non-AEC and right panel corresponds to results with AEC method. The volume of optic radiation in each subject is the mean of both hemispheres. Most observed differences between the OR volumes in the two sequences are within mean  $\pm 1.96 \text{ SD}$ . Middle line indicate mean differences and dashed lines are limits of agreement, defined as mean difference plus (upper line) and minus (lower line) 1.96 SD of differences.

doi:10.1371/journal.pone.0137064.g006

ACT we observed a large number of false positives streamlines projecting to areas outside the visual cortex ([Fig 2a](#)). The use of the top 1% track density threshold in AEC steps was found to be the most convenient to preserve sensitivity and precision by largely reducing false positives voxels (from more than 60% to 17%) rather than increase false negatives (from 3% to 40%) ([S3 Table](#)). Besides, we applied exclusion masks based on anatomical criteria in order to exclude non OR tracks. This was done by excluding streamlines ending in other GM regions apart from the seeds and target masks, as well as CSF and contralateral hemisphere voxels, that did not match with the classical description of the OR anatomy. With the application of AEC steps the accuracy of the streamlines improved in both healthy volunteers and MS patients.

We were able to reconstruct the whole OR, including the Meyer's loop, using only a seed and a target masks that corresponded to the initial and the final part of the tract (the thalamus and the visual cortex, respectively). In comparison with previous reports, we did not require the use of waypoints in the Meyer's loop to reconstruct the part of the tract with higher curvature. The decision to use the whole thalamus as a seed region was made in light of experimental evidence showing that the visual pathway in primates not only connects the LGN with the calcarine cortex but also includes some projections from the pulvinar nuclei in the posterior thalamus [56]. We manually delineated the thalamus to include the LGN, which tended to be systematically missing with FS segmentation [57]. The visual cortex target mask was built by taking the original primary visual cortex FS parcellation (pericalcarine) and merging the surrounding visual association areas (cuneus, lateraloccipital, lingual and precuneus) in order to ensure the inclusion of extrastriate projections of the OR described in humans [58].

To validate the anatomical correspondence of our results in healthy subjects, we created a template of our OR (OR-TCT) and compared it with a histological reference mask, which serves as a gold standard. The comparison of the OR-TCT with histological reference data shows the biological reliability of the tractography framework but also presents some drawbacks that limit the comparison: the histological reference data is based on myelin-stained histological serial sections of 10 human brains and includes the LGNs and the striate GM areas, increasing the size of the template. Since we assume that meaningful tracts only propagate through WM, we excluded GM regions from the histological reference mask when calculating the precision and sensitivity. As such, the differences in precision and sensitivity between both techniques arise not only from the limitation of the tractography algorithm but also from the effect of unavoidable distortions specific to fixation, cutting, staining and mounting of the histological samples. Nevertheless, the accuracy of the results in both HARDI datasets suggested that our OR-TCT matched well with the histological reference data in location and extent (see [Fig 5](#)).

Our study has several strengths. First, the proposed framework was used in different sequences with similar results, demonstrating good reproducibility. We compared the volume of the OR in two HARDI datasets that differ in voxel size and b-value. The results were consistent in both sequences although they presented differences in terms of absolute volume, with higher volumes in the sequence with larger voxel size. Those differences can be related to variations in partial volume effects, contrast in the angular domain and signal-to-noise ratio derived from the different spatial resolutions and b-values [59]. Second, the OR was reconstructed in all MS patients, even in the presence of lesions and microstructural damage. Although the number of patients included was low, the technique appears to be capable of generating a reliable reconstruction of the OR. This can be very useful in the evaluation of the consequences of global and local damage and could be applied to other neurological diseases or for neurosurgical procedures.

However, there are some limitations in the proposed methodology inherent to the technique. First of all, the method is dependent on the seed and target masks positioning, which is the only operator-dependent step and can influence the tractography results. In order to decrease the

probability of bias, the ROIs should be properly segmented to obtain reliable and reproducible positioning. In our study, the automatic segmentation from FS was not suitable so we decided to correct the seed and target masks manually to ensure an accurate reconstruction based on neuro-anatomical knowledge. However, our framework is intended to be used with any selected seed and target masks. Second, this methodology was only evaluated in specific HARDI datasets; therefore, it would be of interest to assess the reliability of OR tracking in higher resolution sequences such as multi-shell HARDI and diffusion spectrum imaging (DSI). Third, the inclusion of the AEC method reduces the sensitivity. This is due in part to exclusion of the most anterior extent of the Meyer's loop streamlines where fibers projecting to the putamen and temporal cortex, not corresponding to the OR, have been described [60]. Despite the decrease in sensitivity, the AEC method increased the precision and accuracy, obtaining an OR reconstruction similar to the histological atlas. Finally, we didn't analyze the presence of damage of the OR in MS patients because our aim was to introduce a reliable tractography methodology. Further clinical studies with higher number of subjects allowing the analysis of changes in MS patients and longitudinal evaluations to assess the reproducibility of the technique are advisable.

## Conclusion

We present a framework for tractography reconstruction that was able to reconstruct the OR with high accuracy and reliability by combining high order probabilistic fiber tracking derived from CSD and automatic post-processing based on anatomical exclusion criteria. Moreover, this technique was applied to different HARDI datasets with equivalent results. Finally, despite the presence of WM damage, it was possible to reconstruct the OR in patients with MS. This framework could be used to accurately represent other tracts with complex configuration and in pathologies affecting the WM.

## Supporting Information

**S1 File. OR-TCT.** Optic radiation tractography-constructed template in both HARDI datasets. The OR obtained in each HARDI dataset was converted into a template. To do so, each individual track density image was aligned to the highest resolution sequence (HARDI A) and was normalized into MNI152 space at 1mm. The “S1 File” is composed by the OR reconstruction in both HARDI datasets in binarized masks.

(ZIP)

**S1 Table. Comparison between tractography results and histological reference data in MS patients.**

(PDF)

**S2 Table. Comparison between the application or not of the AEC method.**

(PDF)

**S3 Table. Comparison between the application or not of the top 1% track density threshold in AEC steps.**

(PDF)

## Acknowledgments

We would like to thank the Medical Imaging Platform at Institut d'Investigacions Biomediques August Pi i Sunyer (IDIBAPS) for the support in image acquisition. The authors thank César Garrido and Dr. Núria Bargalló for their contribution to the design of the acquisition protocol. Vesna Prckovska is a recipient of the FP7 Marie Curie Intra-European Fellowship.

## Author Contributions

Conceived and designed the experiments: EMH VP MA APG SL. Performed the experiments: EMH FV VP CL MA EHM AC APG SL. Analyzed the data: EMH AC FV VP CL MA EHM PV AS APG SL. Contributed reagents/materials/analysis tools: CL MA EHM PV AS. Wrote the paper: EMH FV VP CL MA EHM AC PV EL AS APG SL.

## References

1. Basser PJ, Mattiello J, LeBihan D. MR diffusion tensor spectroscopy and imaging. *Biophysical journal*. 1994 Jan; 66(1):259–67. Available from: <http://www.pubmedcentral.nih.gov/articlerender.fcgi?artid=1275686&tool=pmcentrez&rendertype=abstract> doi: [10.1016/S0006-3495\(94\)80775-1](https://doi.org/10.1016/S0006-3495(94)80775-1) PMID: [8130344](#)
2. Basser PJ, Pajevic S, Pierpaoli C, Duda J, Aldroubi A. In vivo fiber tractography using DT-MRI data. *Magnetic resonance in medicine: official journal of the Society of Magnetic Resonance in Medicine / Society of Magnetic Resonance in Medicine*. 2000 Oct; 44(4):625–32. Available from: <http://www.ncbi.nlm.nih.gov/pubmed/11025519> doi: [10.1002/1522-2594\(200010\)44:4%3C625::AID-MRM17%3E3.0.CO;2-O](https://doi.org/10.1002/1522-2594(200010)44:4%3C625::AID-MRM17%3E3.0.CO;2-O)
3. Hua K, Zhang J, Wakana S, Jiang H, Li X, Reich DS, et al. Tract probability maps in stereotaxic spaces: analyses of white matter anatomy and tract-specific quantification. *NeuroImage*. 2008 Jan; 39(1):336–47. Available from: <http://www.pubmedcentral.nih.gov/articlerender.fcgi?artid=2724595&tool=pmcentrez&rendertype=abstract> doi: [10.1016/j.neuroimage.2007.07.053](https://doi.org/10.1016/j.neuroimage.2007.07.053) PMID: [17931890](#)
4. Mori S, Oishi K, Faria AV. White matter atlases based on diffusion tensor imaging. *Current opinion in neurology*. 2009 Aug; 22(4):362–9. Available from: <http://www.pubmedcentral.nih.gov/articlerender.fcgi?artid=2883814&tool=pmcentrez&rendertype=abstract> doi: [10.1097/WCO.0b013e32832d954b](https://doi.org/10.1097/WCO.0b013e32832d954b) PMID: [19571751](#)
5. Lawes INC, Barrick TR, Murugam V, Spierings N, Evans DR, Song M, et al. Atlas-based segmentation of white matter tracts of the human brain using diffusion tensor tractography and comparison with classical dissection. *NeuroImage*. 2008 Jan; 39(1):62–79. Available from: <http://www.ncbi.nlm.nih.gov/pubmed/17919935> doi: [10.1016/j.neuroimage.2007.06.041](https://doi.org/10.1016/j.neuroimage.2007.06.041) PMID: [17919935](#)
6. Thiebaut de Schotten M, Ffytche DH, Bizzi A, Dell'Acqua F, Allin M, Walshe M, et al. Atlasing location, asymmetry and inter-subject variability of white matter tracts in the human brain with MR diffusion tractography. *NeuroImage*. 2011 Jan; 54(1):49–59. Available from: <http://www.ncbi.nlm.nih.gov/pubmed/20682348> doi: [10.1016/j.neuroimage.2010.07.055](https://doi.org/10.1016/j.neuroimage.2010.07.055) PMID: [20682348](#)
7. Craddock RC, Jbabdi S, Yan CG, Vogelstein JT, Castellanos FX, Di Martino A, et al. Imaging human connectomes at the macroscale. *Nature methods*. 2013 Jun; 10(6):524–39. Available from: <http://www.nature.com/nmeth/journal/v10/n6/full/nmeth.2482.html?message-global=remove> doi: [10.1038/nmeth.2482](https://doi.org/10.1038/nmeth.2482) PMID: [23722212](#)
8. Tuch DS, Reese TG, Wiegell MR, Makris N, Belliveau JW, Wedeen VJ. High angular resolution diffusion imaging reveals intravoxel white matter fiber heterogeneity. *Magnetic resonance in medicine: official journal of the Society of Magnetic Resonance in Medicine / Society of Magnetic Resonance in Medicine*. 2002 Oct; 48(4):577–82. Available from: <http://www.ncbi.nlm.nih.gov/pubmed/12353272> doi: [10.1002/mrm.10268](https://doi.org/10.1002/mrm.10268)
9. Jones DK. Diffusion MRI: Theory, Methods, and Applications. 2010; Available from: [http://books.google.es/books/about/Diffusion\\_MRI\\_Theory\\_Methods\\_and\\_Applica.html?id=dbZCMepD52AC&pgis=1](http://books.google.es/books/about/Diffusion_MRI_Theory_Methods_and_Applica.html?id=dbZCMepD52AC&pgis=1)
10. Bastiani M, Shah NJ, Goebel R, Roebroeck A. Human cortical connectome reconstruction from diffusion weighted MRI: the effect of tractography algorithm. *NeuroImage*. 2012 Sep; 62(3):1732–49. Available from: <http://www.ncbi.nlm.nih.gov/pubmed/22699045> doi: [10.1016/j.neuroimage.2012.06.002](https://doi.org/10.1016/j.neuroimage.2012.06.002) PMID: [22699045](#)
11. Lazar M, Weinstein DM, Tsuruda JS, Hasan KM, Arfanakis K, Meyerand ME, et al. White matter tractography using diffusion tensor deflection. *Human brain mapping*. 2003 Apr; 18(4):306–21. Available from: <http://www.ncbi.nlm.nih.gov/pubmed/12632468> doi: [10.1002/hbm.10102](https://doi.org/10.1002/hbm.10102) PMID: [12632468](#)
12. Behrens TEJ, Berg HJ, Jbabdi S, Rushworth MFS, Woolrich MW. Probabilistic diffusion tractography with multiple fibre orientations: What can we gain? *NeuroImage*. 2007 Jan; 34(1):144–55. Available from: <http://www.ncbi.nlm.nih.gov/pubmed/17070705> doi: [10.1016/j.neuroimage.2006.09.018](https://doi.org/10.1016/j.neuroimage.2006.09.018) PMID: [17070705](#)
13. Farquharson S, Tournier JD, Calamante F, Fabinyi G, Schneider-Kolsky M, Jackson GD, et al. White matter fiber tractography: why we need to move beyond DTI. *Journal of Neurosurgery*. 2013 Jun; 118(6):1367–1377. Available from: [http://thejns.org/doi/abs/10.3171/2013.2.JNS121294?url\\_ver=Z39.88-](http://thejns.org/doi/abs/10.3171/2013.2.JNS121294?url_ver=Z39.88-)

- [2003&rfr\\_id=ori:rid:crossref.org&rfr\\_dat=cr\\_pub%3dpubmed](#) doi: [10.3171/2013.2.JNS121294](https://doi.org/10.3171/2013.2.JNS121294)  
PMID: [23540269](#)
14. Schreiber J, Riffert T, Anwander A, Knösche TR. Plausibility Tracking: a method to evaluate anatomical connectivity and microstructural properties along fiber pathways. *NeuroImage*. 2014 Apr; 90:163–78. Available from: <http://www.sciencedirect.com/science/article/pii/S1053811914000068> doi: [10.1016/j.neuroimage.2014.01.002](https://doi.org/10.1016/j.neuroimage.2014.01.002) PMID: [24418503](#)
15. Tournier JD, and A Connelly FC. Improved probabilistic streamlines tractography by 2nd order integration over fibre orientation distributions. ISMRM. 2010; Available from: <http://www.mendeley.com/catalog/improved-probabilistic-streamlines-tractography-2-nd-order-integration-fibre-orientation-distributio/>
16. Jeurissen B, Leemans A, Jones DK, Tournier JD, Sijbers J. Probabilistic fiber tracking using the residual bootstrap with constrained spherical deconvolution. *Human brain mapping*. 2011 Mar; 32(3):461–79. Available from: <http://www.ncbi.nlm.nih.gov/pubmed/21319270> doi: [10.1002/hbm.21032](https://doi.org/10.1002/hbm.21032) PMID: [21319270](#)
17. Smith RE, Tournier JD, Calamante F, Connelly A. Anatomically-constrained tractography: improved diffusion MRI streamlines tractography through effective use of anatomical information. *NeuroImage*. 2012 Sep; 62(3):1924–38. Available from: <http://www.sciencedirect.com/science/article/pii/S1053811912005824> doi: [10.1016/j.neuroimage.2012.06.005](https://doi.org/10.1016/j.neuroimage.2012.06.005) PMID: [22705374](#)
18. Wu W, Rigolo L, O'Donnell LJ, Norton I, Shriver S, Golby AJ. Visual pathway study using in vivo diffusion tensor imaging tractography to complement classic anatomy. *Neurosurgery*. 2012 Mar; 70(1 Suppl Operative):145–56; discussion 156. Available from: <http://www.ncbi.nlm.nih.gov/articlerender.fcgi?artid=3236807&tool=pmcentrez&rendertype=abstract> doi: [10.1227/NEU.0b013e31822efcae](https://doi.org/10.1227/NEU.0b013e31822efcae) PMID: [21808220](#)
19. Sherbondy AJ, Dougherty RF, Napel S, Wandell BA. Identifying the human optic radiation using diffusion imaging and fiber tractography. *Journal of vision*. 2008 Jan; 8(10):12.1–11. Available from: <http://www.ncbi.nlm.nih.gov/articlerender.fcgi?artid=2759943&tool=pmcentrez&rendertype=abstract> doi: [10.1167/8.10.12](https://doi.org/10.1167/8.10.12)
20. Bürgel U, Schormann T, Schleicher A, Zilles K. Mapping of histologically identified long fiber tracts in human cerebral hemispheres to the MRI volume of a reference brain: position and spatial variability of the optic radiation. *NeuroImage*. 1999 Nov; 10(5):489–99. Available from: <http://www.ncbi.nlm.nih.gov/pubmed/10547327> doi: [10.1006/nimg.1999.0497](https://doi.org/10.1006/nimg.1999.0497) PMID: [10547327](#)
21. Catani M, Jones DK, Donato R, Fytche DH. Occipito-temporal connections in the human brain. *Brain: a journal of neurology*. 2003 Sep; 126(Pt 9):2093–107. Available from: <http://www.ncbi.nlm.nih.gov/pubmed/12821517> doi: [10.1093/brain/awg203](https://doi.org/10.1093/brain/awg203)
22. Mandelstam SA. Challenges of the anatomy and diffusion tensor tractography of the Meyer loop. *AJNR American journal of neuroradiology*. 2012 Aug; 33(7):1204–10. Available from: <http://www.ncbi.nlm.nih.gov/pubmed/22422189> doi: [10.3174/ajnr.A2652](https://doi.org/10.3174/ajnr.A2652) PMID: [22422189](#)
23. Lilja Y, Ljungberg M, Starck G, Malmgren K, Rydenhag B, Nilsson DT. Visualizing Meyer's loop: A comparison of deterministic and probabilistic tractography. *Epilepsy research*. 2014 Mar; 108(3):481–90. Available from: <http://www.ncbi.nlm.nih.gov/pubmed/24559840> doi: [10.1016/j.eplepsyres.2014.01.017](https://doi.org/10.1016/j.eplepsyres.2014.01.017) PMID: [24559840](#)
24. Lilja Y, Nilsson DT. Strengths and limitations of tractography methods to identify the optic radiation for epilepsy surgery. Quantitative imaging in medicine and surgery. 2015 Apr; 5(2):288–99. Available from: <http://www.ncbi.nlm.nih.gov/articlerender.fcgi?artid=4379318&tool=pmcentrez&rendertype=abstract> doi: [10.3978/j.issn.2223-4292.2015.01.08](https://doi.org/10.3978/j.issn.2223-4292.2015.01.08) PMID: [25853086](#)
25. Benjamin CFA, Singh JM, Prabhu SP, Warfield SK. Optimization of tractography of the optic radiations. *Human brain mapping*. 2014 Feb; 35(2):683–697. Available from: <http://www.ncbi.nlm.nih.gov/articlerender.fcgi?artid=4083652&tool=pmcentrez&rendertype=abstract> doi: [10.1002/hbm.22204](https://doi.org/10.1002/hbm.22204) PMID: [23225566](#)
26. Clatworthy PL, Williams GB, Acosta-Cabronero J, Jones SP, Harding SG, Johansen-Berg H, et al. Probabilistic tractography of the optic radiations—an automated method and anatomical validation. *NeuroImage*. 2010 Feb; 49(3):2001–12. Available from: <http://www.ncbi.nlm.nih.gov/pubmed/19900564> doi: [10.1016/j.neuroimage.2009.10.083](https://doi.org/10.1016/j.neuroimage.2009.10.083) PMID: [19900564](#)
27. Hofer S, Karaus A, Frahm J. Reconstruction and dissection of the entire human visual pathway using diffusion tensor MRI. *Frontiers in neuroanatomy*. 2010 Jan; 4:15. Available from: <http://www.ncbi.nlm.nih.gov/articlerender.fcgi?artid=2859811&tool=pmcentrez&rendertype=abstract> doi: [10.3389/fnana.2010.00015](https://doi.org/10.3389/fnana.2010.00015) PMID: [20428499](#)
28. Winston GP, Mancini L, Stretton J, Ashmore J, Symms MR, Duncan JS, et al. Diffusion tensor imaging tractography of the optic radiation for epilepsy surgical planning: a comparison of two methods. *Epilepsy research*. 2011 Nov; 97(1-2):124–32. Available from: <http://www.ncbi.nlm.nih.gov/>

- articlerender.fcgi?artid=3223565&tool=pmcentrez&rendertype=abstract doi: [10.1016/j.epilepsyres.2011.07.019](https://doi.org/10.1016/j.epilepsyres.2011.07.019) PMID: [21885257](#)
29. Yogarajah M, Focke NK, Bonelli S, Cercignani M, Acheson J, Parker GJM, et al. Defining Meyer's loop-temporal lobe resections, visual field deficits and diffusion tensor tractography. *Brain: a journal of neurology*. 2009 Jun; 132(Pt 6):1656–68. Available from: <http://www.ncbi.nlm.nih.gov/pmc/articles/PMC2685925/> doi: [10.1093/brain/awp114](https://doi.org/10.1093/brain/awp114)
30. Kolbe S, Bajraszewski C, Chapman C, Nguyen T, Mitchell P, Paine M, et al. Diffusion tensor imaging of the optic radiations after optic neuritis. *Human brain mapping*. 2012 Sep; 33(9):2047–61. Available from: <http://www.ncbi.nlm.nih.gov/pmc/articles/PMC345943/> doi: [10.1002/hbm.21343](https://doi.org/10.1002/hbm.21343) PMID: [21915943](#)
31. Hodaie M, Quan J, Chen DQ. In vivo visualization of cranial nerve pathways in humans using diffusion-based tractography. *Neurosurgery*. 2010 Apr; 66(4):788–95; discussion 795–6. Available from: <http://www.ncbi.nlm.nih.gov/pmc/articles/PMC20305498/> doi: [10.1227/01.NEU.0000367613.09324.DA](https://doi.org/10.1227/01.NEU.0000367613.09324.DA) PMID: [20305498](#)
32. Sherbondy AJ, Dougherty RF, Ben-Shachar M, Napel S, Wandell BA. ConTrack: Finding the most likely pathways between brain regions using diffusion tractography. *Journal of Vision*. 2008 Jul; 8(9):15–15. Available from: <http://www.ncbi.nlm.nih.gov/pmc/articles/PMC2696074/> doi: [10.1167/8.9.15](https://doi.org/10.1167/8.9.15) PMID: [18831651](#)
33. Tax CMW, Duits R, Vilanova A, ter Haar Romeny BM, Hofman P, Wagner L, et al. Evaluating contextual processing in diffusion MRI: application to optic radiation reconstruction for epilepsy surgery. *PloS one*. 2014 Jan; 9(7):e101524. Available from: <http://journals.plos.org/plosone/article?id=10.1371/journal.pone.0101524> PMID: [25077946](#)
34. Girard G, Whittingstall K, Deriche R, Descoteaux M. Towards quantitative connectivity analysis: reducing tractography biases. *NeuroImage*. 2014 May; 98C:266–278. Available from: <http://www.ncbi.nlm.nih.gov/pmc/articles/PMC4816531/> doi: [10.1016/j.neuroimage.2014.04.074](https://doi.org/10.1016/j.neuroimage.2014.04.074)
35. Gabilondo In, Martínez-Lapiscina EH, Martínez-Heras E, Fraga-Pumar E, Llufriu S, Ortiz S, et al. Trans-synaptic axonal degeneration in the visual pathway in multiple sclerosis. *Annals of neurology*. 2014 Jan; 75(1):98–107. Available from: <http://www.ncbi.nlm.nih.gov/pmc/articles/PMC24114885/> doi: [10.1002/ana.24030](https://doi.org/10.1002/ana.24030) PMID: [24114885](#)
36. Llufriu S, Martínez-Heras E, Fortea J, Blanco Y, Berenguer J, Gabilondo In, et al. Cognitive functions in multiple sclerosis: impact of gray matter integrity. *Multiple sclerosis (Hounds Mills, Basingstoke, England)*. 2014 Apr; 20(4):424–32. Available from: <http://www.ncbi.nlm.nih.gov/pmc/articles/PMC4005025/> doi: [10.1177/1352458513503722](https://doi.org/10.1177/1352458513503722)
37. Rocca MA, Mesaros S, Preziosa P, Pagani E, Stosic-Opincal T, Dujmovic-Basuroski I, et al. Wallerian and trans-synaptic degeneration contribute to optic radiation damage in multiple sclerosis: a diffusion tensor MRI study. *Multiple sclerosis (Hounds Mills, Basingstoke, England)*. 2013 Oct; 19(12):1610–7. Available from: <http://www.ncbi.nlm.nih.gov/pmc/articles/PMC23572238/> doi: [10.1177/1352458513485146](https://doi.org/10.1177/1352458513485146)
38. Martínez-Lapiscina EH, Ortiz-Pérez S, Fraga-Pumar E, Martínez-Heras E, Gabilondo In, Llufriu S, et al. Colour vision impairment is associated with disease severity in multiple sclerosis. *Multiple sclerosis (Hounds Mills, Basingstoke, England)*. 2014 Jan; Available from: <http://www.ncbi.nlm.nih.gov/pmc/articles/PMC24399824/>
39. Pagani E, Filippi M, Rocca MA, Horsfield MA. A method for obtaining tract-specific diffusion tensor MRI measurements in the presence of disease: application to patients with clinically isolated syndromes suggestive of multiple sclerosis. *NeuroImage*. 2005 May; 26(1):258–65. Available from: <http://www.ncbi.nlm.nih.gov/pmc/articles/PMC15862226/> doi: [10.1016/j.neuroimage.2005.01.008](https://doi.org/10.1016/j.neuroimage.2005.01.008) PMID: [15862226](#)
40. Jones DK, Leemans A. Diffusion tensor imaging. *Methods in molecular biology (Clifton, NJ)*. 2011 Jan; 711:127–44. Available from: <http://www.ncbi.nlm.nih.gov/pmc/articles/PMC2127960/> doi: [10.1007/978-1-61737-992-5\\_6](https://doi.org/10.1007/978-1-61737-992-5_6)
41. Desikan RS, Ségonne F, Fischl B, Quinn BT, Dickerson BC, Blacker D, et al. An automated labeling system for subdividing the human cerebral cortex on MRI scans into gyral based regions of interest. *NeuroImage*. 2006 Jul; 31(3):968–80. Available from: <http://www.ncbi.nlm.nih.gov/pmc/articles/PMC16530430/> doi: [10.1016/j.neuroimage.2006.01.021](https://doi.org/10.1016/j.neuroimage.2006.01.021) PMID: [16530430](#)
42. Yushkevich PA, Piven J, Hazlett HC, Smith RG, Ho S, Gee JC, et al. User-guided 3D active contour segmentation of anatomical structures: significantly improved efficiency and reliability. *NeuroImage*. 2006 Jul; 31(3):1116–28. Available from: <http://www.ncbi.nlm.nih.gov/pmc/articles/PMC16545965/> doi: [10.1016/j.neuroimage.2006.01.015](https://doi.org/10.1016/j.neuroimage.2006.01.015) PMID: [16545965](#)
43. Sdika M, Pelletier D. Nonrigid registration of multiple sclerosis brain images using lesion inpainting for morphometry or lesion mapping. *Human brain mapping*. 2009 Apr; 30(4):1060–7. Available from: <http://www.ncbi.nlm.nih.gov/pmc/articles/PMC18412131/> doi: [10.1002/hbm.20566](https://doi.org/10.1002/hbm.20566) PMID: [18412131](#)
44. Jenkinson M. Fast, automated,N-dimensional phase-unwrapping algorithm. *Magnetic Resonance in Medicine*. 2003 Jan; 49(1):193–197. Available from: <http://www.ncbi.nlm.nih.gov/pmc/articles/PMC12509838/> doi: [10.1002/mrm.10354](https://doi.org/10.1002/mrm.10354) PMID: [12509838](#)

45. Greve DN, Fischl B. Accurate and robust brain image alignment using boundary-based registration. *NeuroImage*. 2009 Oct; 48(1):63–72. Available from: <http://www.ncbi.nlm.nih.gov/pmc/articles/PMC2733527/> doi: [10.1016/j.neuroimage.2009.06.060](https://doi.org/10.1016/j.neuroimage.2009.06.060) PMID: [19573611](#)
46. Tournier JD, Calamante F, Connelly A. MRtrix: Diffusion tractography in crossing fiber regions. *International Journal of Imaging Systems and Technology*. 2012 Mar; 22(1):53–66. Available from: <http://doi.wiley.com/10.1002/ima.22005> doi: [10.1002/ima.22005](https://doi.org/10.1002/ima.22005)
47. Alexander DC, Barker GJ, Arridge SR. Detection and modeling of non-Gaussian apparent diffusion coefficient profiles in human brain data. *Magnetic resonance in medicine: official journal of the Society of Magnetic Resonance in Medicine / Society of Magnetic Resonance in Medicine*. 2002 Aug; 48(2):331–40. Available from: <http://www.ncbi.nlm.nih.gov/pmc/articles/PMC12210942/> doi: [10.1002/mrm.10209](https://doi.org/10.1002/mrm.10209)
48. Descoteaux M, Deriche R, Knösche TR, Anwander A. Deterministic and probabilistic tractography based on complex fibre orientation distributions. *IEEE transactions on medical imaging*. 2009 Feb; 28(2):269–86. Available from: <http://www.ncbi.nlm.nih.gov/pmc/articles/PMC19188114/> doi: [10.1109/TMI.2008.2004424](https://doi.org/10.1109/TMI.2008.2004424) PMID: [19188114](#)
49. Dayan M, Munoz M, Jentschke S, Chadwick MJ, Cooper JM, Riney K, et al. Optic radiation structure and anatomy in the normally developing brain determined using diffusion MRI and tractography. *Brain Structure and Function*. 2013 Oct; 220(1):291–306. Available from: <http://www.ncbi.nlm.nih.gov/pmc/articles/PMC4286633/> doi: [10.1007/s00429-013-0655-y](https://doi.org/10.1007/s00429-013-0655-y) PMID: [24170375](#)
50. Klein E, Moeller K, Glauche V, Weiller C, Willmes K. Processing pathways in mental arithmetic—evidence from probabilistic fiber tracking. *PloS one*. 2013 Jan; 8(1):e55455. Available from: <http://www.ncbi.nlm.nih.gov/pmc/articles/PMC3559478/> doi: [10.1371/journal.pone.0055455](https://doi.org/10.1371/journal.pone.0055455)
51. Mori S, Crain BJ, Chacko VP, van Zijl PC. Three-dimensional tracking of axonal projections in the brain by magnetic resonance imaging. *Annals of neurology*. 1999 Feb; 45(2):265–9. Available from: <http://www.ncbi.nlm.nih.gov/pmc/articles/PMC9989633/> doi: [10.1002/1531-8249\(199902\)45:2%3C265::AID-ANA21%3E3.0.CO;2-3](https://doi.org/10.1002/1531-8249(199902)45:2%3C265::AID-ANA21%3E3.0.CO;2-3) PMID: [9989633](#)
52. Fernández-Miranda JC, Rhoton AL, Alvarez-Linera J, Kakizawa Y, Choi C, de Oliveira EP. Three-dimensional microsurgical and tractographic anatomy of the white matter of the human brain. *Neurosurgery*. 2008 Jun; 62(6 Suppl 3):989–1026; discussion 1026–8. Available from: <http://www.ncbi.nlm.nih.gov/pmc/articles/PMC18695585/> PMID: [18695585](#)
53. Bürgel U, Amunts K, Hoemke L, Mohlberg H, Gilsbach JM, Zilles K. White matter fiber tracts of the human brain: three-dimensional mapping at microscopic resolution, topography and intersubject variability. *NeuroImage*. 2006 Feb; 29(4):1092–105. Available from: <http://www.ncbi.nlm.nih.gov/pmc/articles/PMC16236527/> doi: [10.1016/j.neuroimage.2005.08.040](https://doi.org/10.1016/j.neuroimage.2005.08.040) PMID: [16236527](#)
54. Altman DG, Bland JM. Measurement in Medicine: The Analysis of Method Comparison Studies. *The Statistician*. 1983 Sep; 32(3):307. Available from: <http://www.jstor.org/stable/2987937?origin=crossref> doi: [10.2307/2987937](https://doi.org/10.2307/2987937)
55. Kovalev VA, Kruggel F, von Cramon DY. Gender and age effects in structural brain asymmetry as measured by MRI texture analysis. *NeuroImage*. 2003 Jul; 19(3):895–905. Available from: <http://www.ncbi.nlm.nih.gov/pmc/articles/PMC12880818/> doi: [10.1016/S1053-8119\(03\)00140-X](https://doi.org/10.1016/S1053-8119(03)00140-X) PMID: [12880818](#)
56. Markov NT, Misery P, Falchier A, Lamy C, Vezoli J, Quilodran R, et al. Weight consistency specifies regularities of macaque cortical networks. *Cerebral cortex (New York, NY: 1991)*. 2011 Jun; 21(6):1254–72. Available from: <http://www.ncbi.nlm.nih.gov/pmc/articles/PMC3097985/> doi: [10.1093/cercor/cqz020](https://doi.org/10.1093/cercor/cqz020) PMID: [216236527](#)
57. Smith RE, Tournier JD, Calamante F, Connelly A. The effects of SIFT on the reproducibility and biological accuracy of the structural connectome. *NeuroImage*. 2015 Jan; 104:253–65. Available from: <http://www.ncbi.nlm.nih.gov/pmc/articles/PMC25312774/> doi: [10.1016/j.neuroimage.2014.10.004](https://doi.org/10.1016/j.neuroimage.2014.10.004) PMID: [25312774](#)
58. Alvarez I, Schwarzkopf DS, Clark CA. Extrastriate projections in human optic radiation revealed by fMRI-informed tractography. *Brain structure & function*. 2014 Jun; Available from: <http://www.ncbi.nlm.nih.gov/pmc/articles/PMC42903826/>
59. Kim M, Ronen I, Ugurbil K, Kim DS. Spatial resolution dependence of DTI tractography in human occipito-callosal region. *NeuroImage*. 2006 Sep; 32(3):1243–9. Available from: <http://www.ncbi.nlm.nih.gov/pmc/articles/PMC16861009/> doi: [10.1016/j.neuroimage.2006.06.006](https://doi.org/10.1016/j.neuroimage.2006.06.006) PMID: [16861009](#)
60. Goga C, Türe U. The anatomy of Meyer's loop revisited: changing the anatomical paradigm of the temporal loop based on evidence from fiber microdissection. *Journal of neurosurgery*. 2015 Jan; p. 1–10. Available from: <http://www.ncbi.nlm.nih.gov/pmc/articles/PMC25635481/> doi: [10.1227/NEU.00000000000000574](https://doi.org/10.1227/NEU.00000000000000574)